A New Route toward Semiconductor Nanospintronics: Highly Mn-Doped GaAs Nanowires Realized by Ion-Implantation under Dynamic Annealing Conditions

ARTICLE *in* NANO LETTERS · AUGUST 2011

Impact Factor: 13.59 · DOI: 10.1021/nl2021653 · Source: PubMed

NANO LETTERS

LETTER

pubs.acs.org/NanoLett

A New Route toward Semiconductor Nanospintronics: Highly Mn-Doped GaAs Nanowires Realized by Ion-Implantation under Dynamic Annealing Conditions

Christian Borschel,[*,†] Maria E. Messing,[‡] Magnus T. Borgström,[‡] Waldomiro Paschoal, Jr.,[‡] Jesper Wallentin,[‡] Sandeep Kumar,[‡] Kilian Mergenthaler,[‡] Knut Deppert,[‡] Carlo M. Canali,[§] Håkan Pettersson,[‡,∥] Lars Samuelson,[‡] and Carsten Ronning[†]

[†]Institute for Solid State Physics, Jena University, Max-Wien-Platz 1, 07743 Jena, Germany

[‡]Solid State Physics/The Nanometer Structure Consortium, Lund University, Box 118, SE-221 00 Lund, Sweden

[§]Division of Physics, School of Computer Science, Physics and Mathematics, Linnæus University, 39233 Kalmar-Sweden

[∥]Department of Mathematics, Physics, and Electrical Engineering, Halmstad University, Box 823, SE-301 18, Halmstad, Sweden

Supporting Information

ABSTRACT: We report on highly Mn-doped GaAs nanowires (NWs) of high crystalline quality fabricated by ion beam implantation, a technique that allows doping concentrations beyond the equilibrium solubility limit. We studied two approaches for the preparation of Mn-doped GaAs NWs: First, ion implantation at room temperature with subsequent annealing resulted in polycrystalline NWs and phase segregation of MnAs and GaAs. The second approach was ion implantation at elevated temperatures. In this case, the single-crystallinity of the GaAs NWs was maintained, and crystalline, highly Mn-doped GaAs NWs were obtained. The electrical resistance of such NWs dropped with increasing temperature (activation energy about 70 meV). Corresponding magnetoresistance measurements showed a decrease at low temperatures, indicating paramagnetism. Our findings suggest possibilities for future applications where dense arrays of GaMnAs nanowires may be used as a new kind of magnetic material system.

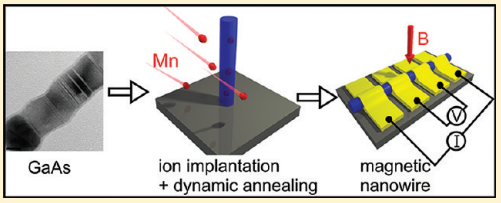

KEYWORDS: Nanowires, GaAs, doping, DMS, ion implantation, dynamic annealing

Ferromagnetic ordering is observed in highly Mn-doped GaAs, in bulk or as thin films, where Mn provides the uncompensated spins as well as p-doping, allowing hole-mediated ferromagnetism. Transition-metal solubility limits in III−V semiconductors are low, but the necessary Mn fractions for ferromagnetic dilute magnetic semiconductors (DMS) can be achieved, for example, by nonequilibrium growth using low temperature MBE at 250 °C.[1] Higher growth temperatures or subsequent annealing typically lead to higher doping levels in the semiconductor, but also segregation into MnAs clusters.[2,3]

Self-assembled semiconductor nanowires (NWs) have proven to be of interest as versatile building blocks of high functionality for various devices, such as field-effect transistors,[4] sensors,[5] and solar cells.[6] Moreover, the small footprint of semiconductor NWs facilitates direct growth on silicon wafers. Dilute magnetic semiconductor NWs would therefore offer a seamless integration of future spintronic devices with mainstream silicon technology, which is one of the main goals of "More than Moore".

Self-organized growth of epitaxial GaAs NWs of high-crystalline quality is possible via metal organic vapor phase epitaxy (MOVPE).[7−9] The relatively high growth temperatures for nanowire growth, typically 400−500 °C, inhibit the homogeneous incorporation of high Mn-concentrations during growth due to the low solubility limit.

Over the years, several attempts have been made to fabricate $Ga_{1-x}Mn_xAs$ NWs. Already in 2002, Sadowski et al. reported the successful growth of InGaMnAs NWs by migration enhanced epitaxy.[10] Later, they established growth of $Ga_{1-x}Mn_xAs$ NWs using MnAs nanoclusters as growth seeds.[11] The obtained NWs contained up to 7% of Mn and were strongly tapered with irregular side facets. The high Mn content led to a branching of the NWs.[12] Martelli et al. performed doping of GaAs NWs using Mn-assisted growth.[13] Recently, Kim et al. synthesized gold-seeded $Ga_{1-x}Mn_xAs$ NWs using a vapor transport method with low Mn content (<5%) exhibiting room-temperature ferromagnetism;[14] however, the magnetic properties are unclear due to lack of any mechanism which could explain the high T_C values.[15] An additional complication is that the Mn may not incorporate homogeneously in the NWs. In fact, it might be that the Mn accumulates in the form of a shell, as indicated by tomographic atom probe measurements for Ge NWs doped during VLS growth.[16] Jeon et al. reported on room-temperature ferromagnetism of GaMnAs NWs with a Mn content of 20%,[17] which is a metallic alloy rather than diluted Mn in a GaAs matrix.

Received: June 27, 2011
Revised: August 12, 2011
Published: August 17, 2011

dx.doi.org/10.1021/nl2021653 | *Nano Lett.* 2011, 11, 3935–3940

Rudolph et al. exploited the possibility to change growth mode from axial to radial nanowire growth and fabricated ferromagnetic GaAs/GaMnAs core/shell NWs.[15] However, the growth of the GaMnAs shell leads to a morphological change from the perfect hexagonal GaAs core NWs toward roughened core/shell GaAs/GaMnAs NWs. A completely different approach was performed by Wolff et al.[18] who decorated GaAs NWs with Mn nanoparticles, which were then transformed into MnAs nanoparticles by thermal annealing in hydrogen and arsine.

Most of the reported attempts suffer from segregation of the MnAs phase during growth leading to nonideal nanowire morphologies. This can easily be exemplified by the morphological change from the perfect hexagonal GaAs core NWs toward totally roughened core/shell NWs after growth of the $Ga_{1-x}Mn_xAs$ shells around them.[15] Furthermore, the detection of segregated MnAs nanoclusters in GaAs with X-ray diffraction (XRD) or high-resolution transmission electron microscopy (HR-TEM) is reported to be rather challenging[19] and these clusters can easily be mistaken for a DMS. In conclusion, in situ Mn-doping of GaAs NWs turns out to be rather difficult to achieve by established growth methods. This observation is well in agreement with the phase diagram determined by Ohno for $Ga_{1-x}Mn_xAs$ layer growth via MBE:[20] For x in the order of 0.5−6%, MnAs forms above about 300 °C.

Postgrowth ion beam implantation is a nonequilibrium doping method that allows concentrations beyond solubility limits and is independent from the growth method of the crystal. It is a standard method for doping of large scale wafers in industry, but it has also been successfully applied for doping of semiconductor NWs.[21] The successful p-doping of GaAs NWs via ion beam implantation of Zn and subsequent annealing at 800 °C under tertiarybutylarsine atmosphere has been reported.[22] Ion beam implantation introduces defects in the target, making postimplantation annealing a necessity. For Mn-implanted GaAs thin films, standard thermal annealing (650 °C) has been reported to lead to MnAs cluster formation.[23] Only pulsed laser melting[24,25] and ion beam-induced epitaxial crystallization annealing[26] have shown promising results regarding the incorporation of Mn in GaAs to create DMS systems.

The annealing methods from bulk cannot directly be transferred to nanosized objects, because, due to their large surface-to-volume ratio, the equilibrium phases strongly differ from those for bulk material. For example, NWs exhibit lower melting points compared to their bulk counterparts.

In this Letter, we compare two approaches for preparation of Mn-doped GaAs NWs by (a) ion implantation at room temperature with subsequent annealing and (b) ion implantation at elevated temperatures making use of in situ dynamic annealing. Furthermore, we report on magnetotransport measurements that were done in order to study the magnetic properties of the implanted $Ga_{1-x}Mn_xAs$ NWs.

Single crystalline, epitaxial GaAs NWs were grown via MOVPE using monodisperse Au particles as catalyst. Details have been published elsewhere.[27] In order to optimize the implantation angle, the NWs were grown on GaAs(001) substrates leading to an inclined growth direction of 35° toward the substrate.[28] NWs were implanted with Mn ions using a general purpose implanter (High Voltage Engineering Europa). Implantation energies of typically 40−60 keV were selected. Results from computer simulations of the ion beam implantation show that these energies lead to a reasonably homogeneous concentration of Mn in the GaAs NWs. Frequently, these simulations

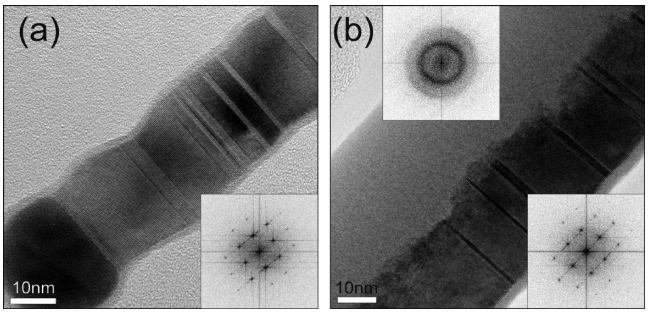

Figure 1. (a) HR-TEM image of an as-grown GaAs nanowire, with the FFT shown in the inset. (b) TEM micrograph of an implanted, nonannealed nanowire (with approx 2.5% Mn), that is partly amorphized and partly crystalline. The two insets show FFTs of the amorphous and crystalline parts, respectively.

are carried out with the widely used SRIM program.[29] However, SRIM assumes flat sample geometry and cannot accurately describe the distribution of implanted ions in NWs. Therefore, we used the new in-house developed code *iradina*,[30] which correctly takes into account the nanowire geometry.

NWs were implanted with Mn doses of 2×10^{15} to 1×10^{16} ions/cm^2 resulting in total Mn concentrations from 0.5 to 2.9% (corresponding to a stoichiometry of $Ga_{1-x}Mn_xAs$ with x from $x = 0.01$ to $x = 0.058$) as calculated with the *iradina* code. Detailed simulation results comparing SRIM and iradina for the given situation are shown in the Supporting Information Figure 1. The first set of samples (a) was implanted at room temperature and subsequently annealed for 30 min either under vacuum at temperatures up to 500 °C, or under AsH_3 atmosphere (molar fraction of 2.20×10^{-3}) from 350 to 650 °C. The second set of samples (b) was implanted at elevated temperatures ranging from 100 to 350 °C. The NWs were characterized by transmission electron microscopy (TEM) using a Jeol 3010 and a Jeol 3000F microscope. The Mn concentration was monitored via X-ray energy dispersive spectroscopy (XEDS).

For magnetotransport measurements, NWs were mechanically transferred onto a silicon substrate covered by a 210 nm thick silicon dioxide layer on which reference markers and macroscopic metal pads were predefined. Prior to transferring of the NWs, trenches were etched in the SiO_2 layer to align the wires for magnetotransport studies. Electron beam lithography was used to define contacts connecting individual NWs to the macroscopic contact pads. The samples were treated in HCl/H_2O solution for 15 s followed by a 2 min surface passivation in a heated (40 °C) NH_4S_x/H_2O solution. To investigate the influence of the contact resistance, 4 Pd(10 nm)/Zn(10 nm)/Pd(35 nm) contacts were evaporated on each NW after passivation.[31] The sample processing was finalized by a lift-off process. The magnetotransport measurements were performed in a Janis VariTemp superconducting cryomagnet system (Model 8T-SVM).

Figure 1a shows an HR-TEM micrograph of a typical nonimplanted, as-grown, NW for comparison. The single-crystalline NWs of zinc blende (ZB) structure were grown in the ⟨111⟩ direction and exhibit twin planes perpendicular to the growth direction, as commonly observed for III−V semiconductor NWs.[32] Resulting from the implantation parameters at room temperature, the NWs were mostly amorphized, which is illustrated in Figure 1b. Depending on the Mn dose, the ion energy, and the exact diameter of the NWs, some parts that face away

dx.doi.org/10.1021/nl2021653 |*Nano Lett.* 2011, 11, 3935–3940

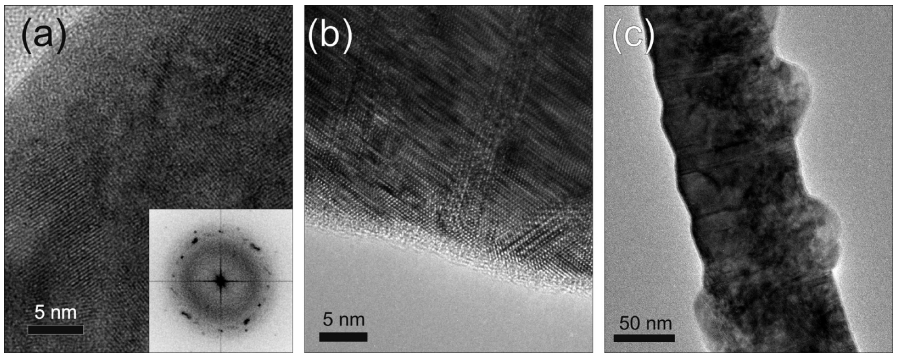

Figure 2. TEM micrographs of implanted and annealed NWs. (a) After annealing in vacuum at 400 °C, the FFT in the inset shows that the nanowire is not single crystalline. (b,c) After annealing in As atmosphere at 550 °C. (b) Nanowire is polycrystalline. (c) Bumps appear on nanowire, consisting of GaAs.

from the ion beam however remained crystalline as illustrated by the fast Fourier transform (FFT) diffraction pattern (inset in Figure 1b).

The NWs recrystallized under annealing in vacuum up to 400 °C, however not to single crystals. A typical polycrystalline nanowire is described by the HR-TEM image and its FFT pattern in Figure 2a. After annealing in vacuum at 500 °C or higher temperatures, we observed that the NWs disappeared, which we interpret as a temperature-induced decomposition of the GaAs NWs, mainly due to the high equilibrium As vapor pressure over GaAs. Therefore, annealing in AsH_3 atmosphere, as previously used to recrystallize Zn-implanted GaAs NWs,[22] was attempted. Within the investigated parameter space, the present Mn-doped NWs survived the treatment but although some recrystallization occurred, they did not become single crystalline (see Figure 2b). Additionally, they featured "bumps" on the sides, as illustrated in Figure 2c. Analysis of the FFT patterns and XEDS shows that these bumps consist of crystalline GaAs without measurable Mn content; the postimplantation annealing with arsine background pressure seems to initiate unwanted regrowth of crystalline GaAs on the amorphized NW.

At this point, we can conclude that room-temperature implantation and subsequent annealing is not suitable to create single crystalline GaAs NWs with a high Mn concentration under the parameter conditions investigated, neither in vacuum, nor in an arsine atmosphere.

During ion beam implantation, so-called dynamic annealing can occur.[33] Each ion induces a collision cascade in the material, producing a large number of point defects (at the order of 10^3 for the parameters used in this study). Additionally, a high amount of energy is deposited by the incident ion as lattice vibrations in the cascade region. Within this so-called "thermal spike", immediate annihilation of defects can occur. When collision cascades from subsequent ions overlap, defects that were created in the earlier cascade can be annihilated by the following ones. If this dynamic annealing is weak, the damage created by subsequent collision cascades is accumulated and ultimately amorphization of the material will occur, if a large fluence of ions is implanted, as observed in this study. Actually, dynamic annealing is enhanced in NWs compared to bulk[34,35] due to the confined geometry resulting into a slower dissipation of the impact energy. However, this annealing effect is not strong enough at room-temperature implantation of Mn into GaAs NWs, and is thus not able to prevent amorphization: the NWs became amorphous when implanted with x = 1% of Mn. Thus, the crystal orientation

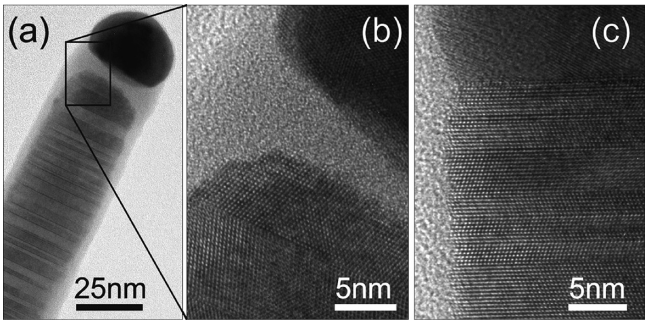

Figure 3. (a) GaAs nanowire implanted with x = 1% Mn at 100 °C. (b) HR image of the same wire showing the amorphous gap between crystalline nanowire core and Au tip. (c) GaAs nanowire implanted with x = 1% Mn at 200 °C.

was lost in the amorphous regions, and subsequent annealing lead to polycrystalline recrystallization, as was described above.

Dynamic annealing can further be enhanced by heating the target during ion implantation[33] due to increased phonon−phonon scattering resulting also into a slower dissipation of the impact energy. In order to make use of this enhanced dynamic annealing, samples were implanted at elevated temperatures. A maximum of 400 °C was used, because decomposition of the GaAs NWs was observed in vacuum at higher temperatures.

Figure 3a,b shows TEM micrographs of a nanowire implanted with Mn at a temperature of 100 °C. A large part of the nanowire remained crystalline during implantation, and the crystalline structure appears similar to the nonimplanted nanowire (Figure 1a). This is in contrast to room-temperature implantation at which the NWs were mostly amorphized. However, an amorphous "neck" close to the catalyst particle appeared after implantation at 100 °C, as illustrated in Figure 3b. This latter observation can be attributed to different efficiency of the dynamic annealing in the proximity of the catalyst particle. For most part of the nanowire, the energy within the thermal spike is sufficient to cause in situ removal of most defects, the crystal orientation is never lost and the material remains single-crystalline in ZB phase and oriented in the (111)B direction. However, when an ion hits the nanowire close to the Au particle, the energy of the thermal spike dissipates much faster, because the thermal conductivity of Au is about 5−6 times larger than of GaAs. Thus, less time is available for annihilation of defects, and amorphization of the material occurs in this area. Such a partial amorphization

dx.doi.org/10.1021/nl2021653 |*Nano Lett.* 2011, 11, 3935–3940

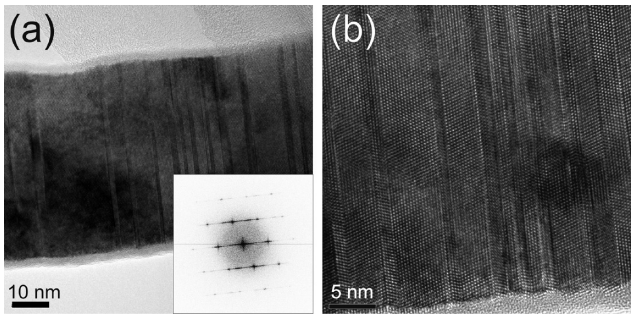

Figure 4. (a) HR-TEM micrograph of GaAs nanowire implanted with x = 5% Mn at 250 °C and FFT of the complete image as inset demonstrating excellent crystalline quality of the Mn-implanted wires. (b) HR-TEM micrograph with higher magnification.

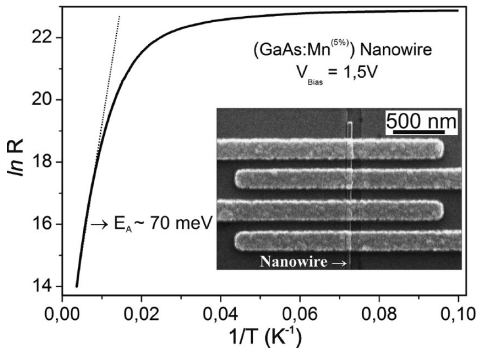

Figure 5. Plot of resistance versus reciprocal temperature with indicated activation energy. The inset shows an SEM micrograph of a nanowire supplied with contacts for 4-point measurements.

could be avoided by further increasing the implantation temperature to above 100 °C. Then, the dynamic annealing was sufficiently enhanced to maintain crystallinity of the complete nanowire, as illustrated for a nanowire implanted at 200 °C in Figure 3c. It should be noted that apart from dynamic annealing caused by the ion beam, normal "thermal healing" may also occur at the higher temperatures in between the ion impacts. However, it is not possible to separate the contributions from ion beam and temperature in the annealing.

From thin film growth of $Ga_{1-x}Mn_xAs$ it is known that phase separation of MnAs occurs above 250−300 °C depending on the Mn concentration.[20] However, due to their small size this limit may be lower for NWs. Therefore, we also examined implantation with high doses of Mn at 250 °C; the results are illustrated in Figure 4a, showing an HR-TEM image of a nanowire implanted with 10^{16} ions/cm^2, corresponding to a total Mn concentration of 2.9% (x = 0.058). Even at these high concentrations, the NWs were observed to remain single-crystalline and no secondary phases were observed. XEDS measurements were performed on several areas on these NWs (Supporting Information Figure 2). They confirmed a Mn concentration of about 2−3%, showing that Mn has not diffused out during implantation at elevated temperatures.

It should be noted at this point, that computer simulations of the ion beam implantation require that the correct nanowire geometry is taken into account. Simulations using SRIM[29] overestimate the implanted concentration of Mn in the NWs by about a factor of 1.7, while simulations using the *iradina* code[30] predict the Mn concentration more accurately to about 2.9%. The reason is that SRIM can only simulate flat targets and therefore cannot take into account ions leaving the nanowire from the sides.

A recovery stage for the electronic properties of GaAs around 250 °C has been reported by Thommen for high-energy electron-beam irradiated GaAs and subsequent annealing.[36] Thus, it seems useful to use at least 250 °C during implantation, although single-crystallinity was already observed at 150 °C. We further increased the implantation temperature to 350 °C and still obtained single crystalline NWs; however, the optimum temperature has to be balanced, since, as mentioned in the introduction, at higher temperatures the precipitation of MnAs nanoclusters becomes more likely.[37] We did not observe MnAs precipitates in the implanted NWs up to 350 °C, but nanometric inclusions of this phase are not easily detectable[19] and cannot be excluded.

Considering the upper and lower limitations, 250 °C was identified as the suitable temperature for creating GaMnAs nanowire with high Mn content via ion beam implantation. This is consistent with the temperature at which Ohno et al. have grown LT-MBE magnetic GaMnAs thin films.[1] Furthermore, 250 °C is also the same temperature Chen et al. used for ion-beam annealing of Mn implanted GaAs thin films.[26]

Transport measurements were carried out between 1.6 and 300 K. To investigate possible influence of contact resistance, 2-point and 4-point measurements were compared down to about 70 K where 4-point measurements became difficult to carry out due to a very high resistance. From these measurements, we conclude that the contact resistance is negligible compared to the NW resistance. The IV-characteristics are in general fairly linear down to about 100 K (Supporting Information Figure 3). At lower temperatures, a symmetrical nonlinear behavior becomes increasingly dominant. Figure 5 displays the resistance of a typical implanted NW versus reciprocal temperature from which we deduce an activation energy of about 70 meV. We have investigated several NWs that all show the same behavior. A similar behavior has previously been reported for planar GaMnAs films and attributed to thermal emission of holes from a Mn impurity band to the valence band.[38] The activation energy is smaller than the typical 100−110 meV observed for weakly doped GaAs:Mn, where the emission originates from isolated Mn impurities.[39] Interestingly, the room-temperature resistance is in the MΩ regime, which is unexpectedly high, considering the nominal x = 5.8% Mn incorporation. A plausible explanation for the apparent low hole concentration ($\sim 10^{17}$ cm^{-3} assuming a reduced mobility of 60 cm^2/(V s)[38] and 40 nm wire diameter) is a Fermi-level pinning at the GaAs surface, which effectively creates a radially depleted semiconductor wire. Also, most likely compensation occurs due to incorporation of interstitial Mn and substitutional As_{Ga} antisites, both acting as double donors. The resulting hole concentration is too low to create the necessary effective ferromagnetic coupling between Mn spins, which results in a paramagnetic state rather than in ferromagnetic ordering. The absence of the onset of any ferromagnetic order in our sample is also evident from the lack of any singularity in the derivative of the resistance as a function of temperature in the range of temperatures (40−190 K), which is expected to occur at the critical temperature.[40] Further understanding of the magnetic state of our implanted wires is obtained from magnetoresistance (MR) studies. In Figure 6, we plot the MR as a function of an external magnetic field applied in the direction parallel and perpendicular to the wire. The data readily shows a negative MR signal up to about 50 K. No evident trace of

dx.doi.org/10.1021/nl2021653 |*Nano Lett.* 2011, 11, 3935–3940

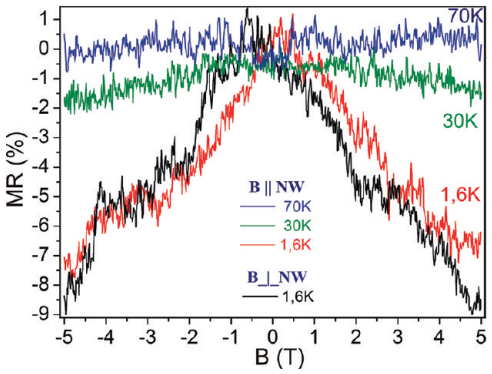

Figure 6. Plot of magnetoresistance versus temperature for parallel (∥) and perpendicular (⊥) orientation of magnetic field relative to nanowire (only one sweep direction is shown).

hysteresis effects was found in our measurements and additionally, the MR does not seem to saturate (up to 5 T). There is also no clear indication of any anisotropic MR changes at small magnetic fields that typically occur in ferromagnetic DMS due to reorientation of the magnetization relative to the current direction. While these MR results support the conclusion that our samples are not ferromagnetic, they are also a strong indication of a paramagnetic state of the system due to the presence of Mn impurities. Indeed, nonimplanted NWs display dramatically different electrical properties with very high resistance (∼200 GΩ) already at room temperature, which makes magnetotransport measurements virtually impossible. Negative MR traces are normally attributed to spin-disorder scattering in metallic samples[20] and to suppression of Anderson localization of holes in insulating or semiconducting samples.[41] Possibly, in the regime of low conductance of our sample, both mechanisms are contributing to some extent in reducing the resistance. The observed MR effect may reflect a decrease in resistance as a result of a Zeeman shift of the Fermi energy toward the Anderson mobility edge by the applied magnetic field, which furthermore reduces spin-disorder scattering by successively aligning the randomly oriented individual Mn spins along its direction. The Zeeman energy for a spin 5/2 is of the order of 20 K at 5 T. If we assume that the magnetization of the sample at a given temperature and magnetic field is proportional to the Brillouin function, the magnetization and consequently the MR should reach saturation at fields on the order of 8 T when the temperature is 1.6 K. On the other hand, as shown in Figure 6, at temperatures above 70 K and at a magnetic field of 5 T, the thermal energy totally randomizes the spin orientation which consequently quenches the MR.

The MR curves further indicate that the Mn is mainly diluted in the GaAs host and not incorporated in the form of ferromagnetic MnAs clusters; Michel et al. have theoretically studied the influence of ferromagnetic MnAs clusters in a paramagnetic GaMnAs host matrix on the MR behavior.[42] They find that a high density of MnAs clusters leads to a strong negative MR below 30 K and a very strong positive MR of several hundred percent between 30 and 100 K. The Mn-doped nanowires only show a weak negative MR below 70 K and no MR at higher temperatures, indicating that there are either no MnAs clusters or at least a very low density of them.

In conclusion, we have realized high-crystalline quality Mn-doped GaAs NWs via ion beam implantation, which allows incorporation of dopants into the target material far beyond the solubility limit. In order to minimize ion beam-induced defects different annealing routes were investigated. Postannealing was not successful for NWs, because the NWs either decomposed or became polycrystalline within the investigated parameter space. However, heating the sample to higher temperatures during implantation (250 °C) enabled increased dynamic annealing in addition to thermal healing, resulting in single-crystalline $Ga_{1-x}Mn_xAs$ NWs with high Mn content.

We also report on magnetotransport measurements on the Mn-implanted NWs, where a strong-temperature dependence of the resistance was observed in addition to a clear negative MR at low temperatures. These results indicate dilute Mn incorporation and, in combination with the observed high resistance of the NWs, support the hypothesis that the implanted NWs are paramagnetic due to a strong reduction in free hole concentration that stems from surface pinning effects and, possibly, from Mn interstitials and As_{Ga} antisites.

This study provides the groundwork to pursue further ion-implantation experiments, for example, in thicker NWs, and to develop novel technology for tuning the hole concentration in the NWs to facilitate an electrically controlled hole concentration and thus ferromagnetism. We believe that the work presented here demonstrates a promising route for future fabrication of complex integrated DMS nanostructures, where arrays of Mn-doped NWs may be functioning as a novel kind of material system for science as well as for applications.

■ ASSOCIATED CONTENT

Supporting Information. Additional information and figures. This material is available free of charge via the Internet at http://pubs.acs.org.

■ AUTHOR INFORMATION

Corresponding Author
*E-mail: christian.borschel@uni-jena.de.

■ ACKNOWLEDGMENT

We acknowledge support by the Swedish Research Council under Grant Number: 621-2010-3761.

■ REFERENCES

(1) Ohno, H.; Shen, A.; Matsukura, F.; Oiwa, A.; Endo, A.; Katsumoto, S.; Iye, Y. *Appl. Phys. Lett.* **1996**, *69*, 363.
(2) De Boeck, J.; Oesterholt, R.; Bender, H.; Van Esch, A.; Bruynseraede, C.; Van Hoof, C.; Borghs, G. *J. Magn. Magn. Mater.* **1996**, *156*, 148.
(3) Wellmann, P. J.; Garcia, J. M.; Feng, J.-L.; Petroff, P. M. *Appl. Phys. Lett.* **1997**, *71*, 2532.
(4) Cui, Y.; Zhong, Z.; Wang, D.; Wang, W. U.; Lieber, C. M. *Nano Lett.* **2003**, *3*, 149.
(5) Yeh, P.-H.; Li, Z.; Wang, Z. L. *Adv. Mater.* **2009**, *21*, 4975.
(6) Hochbaum, A. I.; Yang, P. *Chem. Rev.* **2010**, *110*, 527.
(7) Borgström, M.; Deppert, K.; Samuelson, L.; Seifert, W. *J. Cryst. Growth* **2004**, *260*, 18.
(8) Wagner, R. S.; Ellis, W. C. *Appl. Phys. Lett.* **1964**, *4*, 89.
(9) Wacaser, B. A.; Dick, K. A.; Johansson, J.; Borgström, M. T.; Deppert, K.; Samuelson, L. *Adv. Mater.* **2009**, *21*, 153–165.
(10) Sadowski, J.; Deppert, K.; Kanski, V.; Ohlsson, J.; Persson, A.; Samuelson, L. *Proceedings of the 7th International Conference on Nanometer-scale Science and Technology*, June 24−28, Malmö, Sweden, 2002.

(11) Sadowski, J.; Dłużewski, P.; Kret, S.; Janik, E.; Łusakowska, E.; Kanski, J.; Presz, A.; Terki, F.; Charar, S.; Tang, D. *Nano Lett.* **2007**, *7*, 2724.
(12) Dluzewski, P.; Sadowski, J.; Kret, S.; Dabrowski, J.; Sobczak, K. *J. Microsc.* **2009**, *236*, 115.
(13) Martelli, F.; Rubini, S.; Piccin, M.; Bais, G.; Jabeen, F.; Franceschi, S. D.; Grillo, V.; Carlino, E.; D'Acapito, F.; Boscherini, F.; Cabrini, S.; Lazzarino, M.; Businaro, L.; Romanato, F.; Franciosi, A. *Nano Lett.* **2006**, *6*, 2130.
(14) Kim, H. S.; Cho, Y. J.; Kong, K. J.; Kim, C. H.; Chung, G. B.; Park, J. *Chem. Mater.* **2009**, *21*, 1137.
(15) Rudolph, A.; Soda, M.; Kiessling, M.; Wojtowicz, T.; Schuh, D.; Wegscheider, W.; Zweck, J.; Back, C.; Reiger, E. *Nano Lett.* **2009**, *9*, 3860.
(16) Perea, D. E.; Hemesath, E. R.; Schwalbach, E. J.; Lensch-Falk, J. L.; Voorhees, P. W.; Lauhon, L. J. *Nat. Nanotechnol.* **2009**, *4*, 315.
(17) Jeon, H. C.; Kang, T. W.; Kim, T. W.; Yu, Y.-J.; Jhe, W.; Song, S. A. *J. Appl. Phys.* **2007**, *101*, 023508.
(18) Wolff, M. F. H.; Görlitz, D.; Nielsch, K.; Messing, M. E.; Deppert, K. *Nanotechnology* **2011**, *22*, 055602.
(19) Seo, S. S. A.; Noh, T. W.; Kim, Y.-W.; Lim, J. D.; Park, Y. D.; Kim, Y. S.; Khim, Z. G.; Jeon, H. C.; Kang, T. W.; Pearton, S. J. *J. Appl. Phys.* **2004**, *95*, 8172.
(20) Ohno, H. *J. Magn. Magn. Mater.* **1999**, *200*, 110–129.
(21) Ronning, C.; Borschel, C.; Geburt, S.; Niepelt, R. *Mater. Sci. Eng., R* **2010**, *70*, 30.
(22) Stichtenoth, D.; Wegener, K.; Gutsche, C.; Regolin, I.; Tegude, F. J.; Prost, W.; Seibt, M.; Ronning, C. *Appl. Phys. Lett.* **2008**, *92*, 163107.
(23) Bürger, D.; Zhou, S.; Grenzer, J.; Reuther, H.; Anwand, W.; Gottschalch, V.; Helm, M.; Schmidt, H. *Nucl. Instrum. Methods Phys. Res., Sect. B* **2009**, *267*, 1626.
(24) Scarpulla, M. A.; Dubon, O. D.; Yu, K. M.; Monteiro, O.; Pillai, M. R.; Aziz, M. J.; Ridgway, M. C. *Appl. Phys. Lett.* **2003**, *82*, 1251.
(25) Scarpulla, M. A.; Farshchi, R.; Stone, P. R.; Chopdekar, R. V.; Yu, K. M.; Suzuki, Y.; Dubon, O. D. *J. Appl. Phys.* **2008**, *103*, 073913.
(26) Chen, C. H.; Niu, H.; Hsieh, H. H.; Cheng, C. Y.; Yan, D. C.; Chi, C. C.; Kai, J. J.; Wu, S. C. *J. Magn. Magn. Mater.* **2009**, *321*, 1130.
(27) Mikkelsen, A.; Sköld, N.; Ouattara, L.; Borgström, M.; Andersen, J. N.; Samuelson, L.; Seifert, W.; Lundgren, E. *Nat. Mater.* **2004**, *3*, 519–523.
(28) Hiruma, K.; Yazawa, M.; Katsuyama, T.; Ogawa, K.; Haraguchi, K.; Koguchi, M.; Kakibayashi, H. *J. Appl. Phys.* **1995**, *77*, 447.
(29) Ziegler, J. F.; Biersack, J. P.; Littmark, U. *The stopping and ranges of ions in solids*; Pergamon Press: New York, 1985.
(30) Borschel, C.; Ronning, C. *Nucl. Instrum. Methods Phys. Res., Sect. B* **2011**, *269*, 2133.
(31) Wallentin, J.; Persson, J. M.; Wagner, J. B.; Samuelson, L.; Deppert, K.; Borgstrom, M. T. *Nano Lett.* **2010**, *10*, 974–979.
(32) Yazawa, M.; Koguchi, M.; Hiruma, K. *Appl. Phys. Lett.* **1991**, *58*, 1080.
(33) Williams, J. S. *Mate. Sci. Eng.* **1998**, *253*, 8.
(34) Dhara, S.; Datta, A.; Wu, C. T.; Lan, Z. H.; Chen, K. H.; Wang, Y. L.; Chen, L. C.; Hsu, C. W.; Lin, H. M.; Chen, C. C. *Appl. Phys. Lett.* **2003**, *82*, 451.
(35) Colli, A.; Fasoli, A.; Ronning, C.; Pisana, S.; Piscanec, S.; Ferrari, A. C. *Nano Lett.* **2008**, *8*, 2188.
(36) Thommen, K. *Radiat. Eff.* **1970**, *2*, 201.
(37) Ohno, H. *Science* **1998**, *281*, 951.
(38) Slupinski, T.; Caban, J.; Moskalik, K. *Acta Phys. Pol., A* **2007**, *112*, 325–330.
(39) Ilegems, M.; Dingle, R.; Rupp, L. W., Jr. *J. Appl. Phys.* **1975**, *46*, 3059.
(40) Novák, V.; Olejník, K.; Wunderlich, J.; Cukr, M.; Výborný, K.; Rushforth, A. W.; Edmonds, K. W.; Campion, R. P.; Gallagher, B. L.; Sinova, J.; Jungwirth, T. *Phys. Rev. Lett.* **2008**, *101*, 077201.
(41) Iye, Y.; Oiwa, A.; Endo, A.; Katsumoto, S.; Matsukura, F.; Shen, A.; Ohno, H.; Munekata, H. *Mater. Sci. Eng., B* **1999**, *63*, 88.
(42) Michel, C.; Elm, M. T.; Goldlücke, B.; Baranovskii, S. D.; Thomas, P.; Heimbrodt, W.; Klar, P. J. *Appl. Phys. Lett.* **2008**, *92*, 223119.